analytical chemistry

Article

pubs.acs.org/ac

Illuminating Superoxide Anion and pH Enhancements in Apoptosis of Breast Cancer Cells Induced by Mitochondrial Hyperfusion Using a New Two-Photon Fluorescence Probe

Wen Zhang, Xin Wang, Ping Li,* Haibin Xiao, Wei Zhang, Hui Wang, and Bo Tang*

College of Chemistry, Chemical Engineering and Materials Science, Collaborative Innovation Center of Functionalized Probes for Chemical Imaging in Universities of Shandong, Key Laboratory of Molecular and Nano Probes, Ministry of Education, Institutes of Biomedical Sciences, Shandong Normal University, Jinan 250014, People's Republic of China

Supporting Information

ABSTRACT: Mitochondrial morphology regulated by fusion and fission processes determines mitochondrial function and cell fate. Some studies showed hyperfused mitochondria could induce apoptosis in cancer cells, but the relevant molecular mechanisms remain elusive. Superoxide ($O_2^{\bullet-}$) and pH play vital roles in mitochondrial dysfunction and apoptosis. Therefore, it is worthwhile to explore if there is an intimate relationship between mitochondrial hyperfusion and simultaneous changes in $O_2^{\bullet-}$ and pH levels, which will be helpful to uncover relevant detailed mechanism. For this purpose, we have developed a new reversible two-photon fluorescent probe (CFT) to simultaneously monitor $O_2^{\bullet-}$ and pH in 4T1 cells and mice using dual-color imaging. With the assistance of probe, we found that inhibition of Dynamin-related protein 1 (Drp1) could transduce a signal through mitochondrial complexes I and II to enhance the $O_2^{\bullet-}$ and pH levels and eventually induced mitohyperfusion and apoptosis in breast cancer cells. Together, these data indicate that CFT provides a robust tool for unveiling the roles of $O_2^{\bullet-}$ and pH in signals associated with mitochondrial dysfunction in cells and *in vivo*.

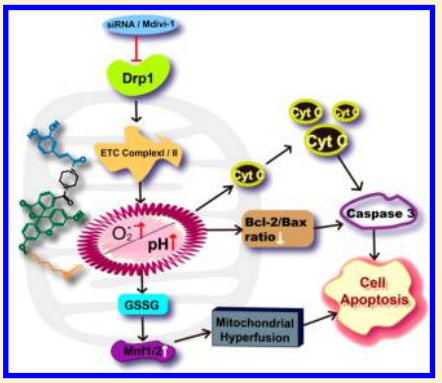

Mitochondria, the powerhouses of the cell, are highly dynamic organelles regulated by coordinated fission and fusion events.[1] These events are controlled by machinery involving large dynamin-related GTPases that exert fission or fusion effects, such as the fission-related Dynamin-related protein 1 (Drp1).[2] Deficiencies in controlling mitochondrial morphology can result in dysfunction, which are associated with a number of pathologies,[3] such as Alzheimer's disease and cancer.[4] Recent study showed that hyperfused mitochondria could induce apoptosis of lung cancer cells.[5] However, the relevant molecular mechanisms behind these observations remain elusive, once we solve the regulatory puzzle, it will be a great help to the treatment of cancer. In the study of mitochondrial dysfunction, superoxide ($O_2^{\bullet-}$) and pH have attracted extensive attention. It is because $O_2^{\bullet-}$ is one of the most important of reactive oxygen species (ROS) and may play a critical role in regulations of mitochondrial morphology and apoptosis.[6−8] Besides some studies have demonstrated that mitochondrial pH have close relations to apoptosis and $O_2^{\bullet-}$ can trigger Na^+/H^+ antiporter inducing a pH increase.[9,10] Probably the concentrations of $O_2^{\bullet-}$ and pH alter synchronously in one checkpoint, which are immensely involved in signal transduction that is regulated by dynamic changes of mitochondria. Therefore, exploring a potential relationship between mitochondrial hyperfusion and synchronous changes in $O_2^{\bullet-}$ and pH levels is helpful to uncover relevant detailed mechanism. For this purpose, a reliable method is needed for simultaneous monitoring $O_2^{\bullet-}$ and pH fluctuations in hyperfused mitochondria.

Fluorescence imaging associated with specific fluorescent probes has been developed to study $O_2^{\bullet-}$ or pH in living systems,[11−13] especially two-photon (TP) fluorescence imaging.[14,15] This approach has the prominent advantages of noninvasiveness,[16] excellent temporal resolution[17] and deep-tissue penetration.[18−21] To explore the instantaneous changes of both $O_2^{\bullet-}$ and pH level in mitohyperfusion, dynamic and reversible fluorescent imaging tools are pressing required. Although we could combine two different fluorescent probes for observing $O_2^{\bullet-}$ and pH, this method may suffer discrepant biological locations and higher toxicity. Therefore, utilizing a simple and stable molecular probe responding to multicomponent can avoid the defects mentioned above and provide more precise and reliable information. However, up to date, the molecular probes possessing performance advantages of dynamic, reversible, and simultaneous response to mitochondrial $O_2^{\bullet-}$ and pH are still lacking.

Thus, to solve this issue, we fabricate a new reversible two-photon fluorescent probe (*N*-(2E)-3-(3,4-dihydroxyphenyl) acrylic acyl)-*N*′-6-carboxyfluorescein-3′-hexyloxy-triphenylphosphonium salts, CFT) comprising covalently linked caffeoyl,

Received: April 6, 2017
Accepted: May 15, 2017
Published: May 15, 2017

DOI: 10.1021/acs.analchem.7b01290
Anal. Chem. 2017, 89, 6840−6845

Scheme 1. Structure and Luminescence Mechanism of CFT

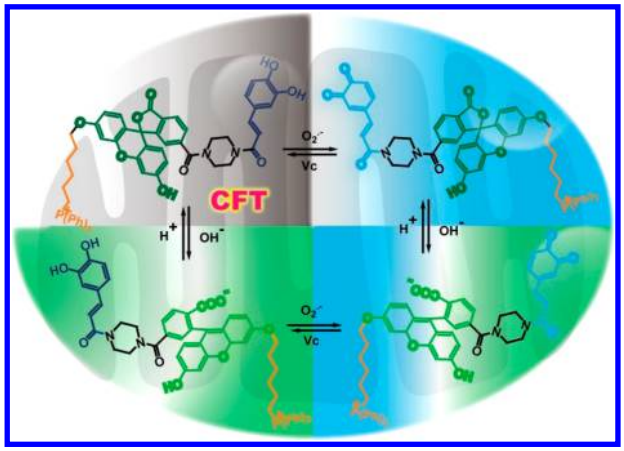

fluorescein, and triphenylphosphonium (Scheme 1). On the basis of our previous work on dynamic detection of $O_2^{\bullet-}$,[22] the caffeoyl moiety is a satisfactory candidate for the $O_2^{\bullet-}$ recognition group. Meanwhile, the fluorescein moiety serves as the pH response group, and cationic triphenylphosphonium is used to target mitochondria.[23,24] Using two sets of distinct blue-green fluorescence signals, the changes in $O_2^{\bullet-}$ or pH levels can be differentiated. CFT was applied to specific, instantaneous, and dynamic detection of mitochondrial $O_2^{\bullet-}$ and pH fluctuations via dual-color fluorescence imaging basing on two-photon single excitation. Furthermore, with the assistance of CFT, we explored the $O_2^{\bullet-}$ and pH signaling pathways regulated by inhibition of Drp1 in breast cancer cells and tumor mice model.

EXPERIMENTAL SECTION

Materials and Reagents. All chemicals were purchased from Adamas Reagent, Ltd. (China) and Energy Chemical, Ltd. (China). Analytical grade solvents were used without further purification. We prepared the reactive oxygen species (ROS) as follows. H_2O_2, hypochlorite (NaOCl), and *tert*-butyl hydroperoxide (TBHP) were used in aqueous solutions of 30%, 10%, and 70%, respectively. Hydroxyl radicals ($^{\bullet}OH$) were generated by the reaction of 1 mM Fe^{2+} with 200 μM H_2O_2. Singlet oxygen ($^1O_2$) was prepared using the ClO^-/H_2O_2 system, and peroxynitrite was created from a stock solution of 10 mM in 0.3 M NaOH. Superoxide ($O_2^{\bullet-}$) was generated from KO_2 in DMSO solution.

Instrumentation. ^{1}HNMR spectra were examined at 400 MHz using Bruker NMR spectrometers. The mass spectra were obtained using the Bruker maXis ultrahigh resolution-TOF MS system. All one-photon fluorescence spectra were measured at room temperature on an FLS-980 Edinburgh fluorescence spectrometer. The two-photon excited fluorescence spectra were measured using a Zeiss LSM 880 NLO.

Cell and Mice Culture. 4T1 cells were cultured in RPMI 1640 supplemented with 10% fetal bovine serum, 1% penicillin, and 1% streptomycin at 37 °C (w/v) in a 5% CO_2 and 95% air incubator MCO-15AC (Sanyo, Tokyo, Japan). One day before imaging, the cells were detached and replanted onto glass-bottomed dishes.

The tumor model used 8- to 10-week-old Balb/c mice (female). The tumor model was established by athoracic injection of 4T1 cells suspensions (10^5 cells mL^{-1}). When the tumor diameter reached 0.5 cm, the tumor-bearing animals were used for analysis.

Fluorescence Imaging. One-photon fluorescent images were acquired on a Leica TCS SP8 confocal laser-scanning microscope with an objective lens (×63 and ×100) and Leica STED microscope (×100). The excitation wavelength was 405 nm (0.5 mW) and 488 nm (4.5 mW). The TP images were acquired with a Zeiss LSM 880 NLO (25× water objective). The Ti:sapphire laser was used to excite the specimen at 800 nm, and the laser power was 70 mW.

Cytotoxicity Assays. We assessed the potential toxicities of CFT against a 4T1 cell line using the MTT {3-(4,5-dimethylthiazol-2-yl)-2,5-diphenyltetrazolium bromide} assay according to the manufacturer's protocol. First, we seeded the 4T1 cells (10^6 cell mL^{-1}) into replicate 96-well microtiter plates at a total volume of 200 μL well^{-1}. After 12 h of culture as previously described, various concentrations of CFT (1×10^{-4}, 1×10^{-5}, 1×10^{-6}, and 1×10^{-7} M) were added to the cells and incubated for 12 h. Subsequently, MTT solution (5 mg mL^{-1}, PBS) was added to each well. The MTT solution was removed after 4 h of incubation, and 150 μL of DMSO was added into each well. Finally, we measured the absorbance at 490 nm in a TRITURUS microplate reader.

RESULTS AND DISCUSSION

The synthesis and absorption spectra of CFT are shown in Figures S1 and S2a,Supporting Information. The one-photon (OP) and TP fluorescence properties of CFT were examined under simulated physiological conditions (30 mM PBS buffer, pH 7.4). As shown in Figure 1, upon single TP excitation

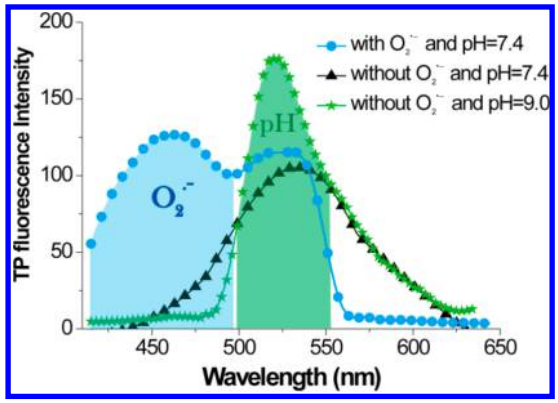

Figure 1. TP emission spectra for CFT (10 μM) before (▲) and after (●) the addition of $O_2^{\bullet-}$ (30 μM) at pH 7.4 and with addition of pH 9.0 PBS buffer (★) at 800 nm excitation.

(800 nm), two distinguishable blue and green fluorescence signals were obtained depending on the changes in $[O_2^{\bullet-}]$ and pH. Upon excitation at 800 nm (TP) or 400 nm (OP, Figure S2b), more intense blue fluorescence (caffeoyl moieties, 450 nm) was observed in the presence of $O_2^{\bullet-}$ (TP cross-section σ = 30.1 GM and fluorescence quantum yield Φ_f = 0.12). Figure S2c,d illustrates the linear relationship between fluorescence intensities and $[O_2^{\bullet-}]$ in a wide range from 10 nM to 30 μM, and the detection limit was 2.8 nM. Similarly, when raising pH values from 5.0 to 9.0, a pronounced enhancement of green fluorescence (fluorescein moiety, 520 nm) was observed under 488 nm excitation (OP, Φ_f = 0.51, Figure S2e), and the plot of fluorescence intensities vs pH over the pH range of 5.0−9.0 is illustrated. These data imply that the recognition sites of caffeoyl and fluorescein can appropriately operate in the presence of $O_2^{\bullet-}$ and pH separately or together via diverse fluorescence signal changes.

DOI: 10.1021/acs.analchem.7b01290
Anal. Chem. 2017, 89, 6840−6845

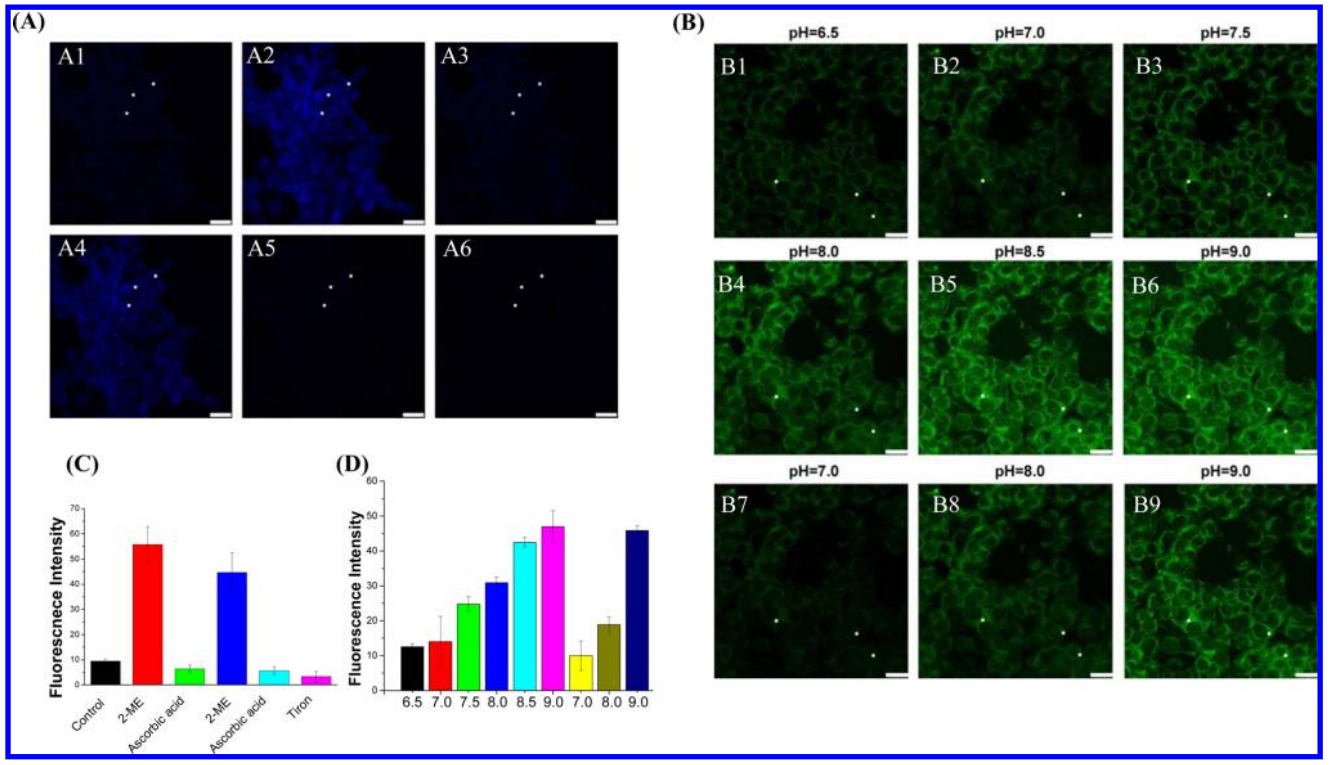

Figure 2. *In situ* fluorescence imaging in 4T1 cells: (A1) cells incubated only with 10 μM CFT for 10 min at room temperature, (A2) cells preincubated with 10 μM CFT were treated with 2-ME (1.0 μg/mL) for 30 min, (A3) cells from part A2 were then incubated with 1.0 mM ascorbic acid for 30 min. (A4) Cells from part A3 were treated with 2-ME (1.0 μg/mL) for 30 min. (A5) Cells from part A4 were incubated with 1.0 mM ascorbic acid for 30 min. (A6) The 2-ME-stimulated cells were incubated with 10 μM Tiron for 30 min before the addition of 10 μM CFT. (B) Confocal fluorescence images of 4T1 cells under pH ranging from 6.0 to 9.0 and then from 7.0 to 9.0. (C, D) Relative fluorescence intensities of CFT-labeled 4T1 cells in white squares in parts A and B. The excitation wavelength of blue fluorescence was excited at 405 nm, and its emission window was 430−480 nm. The excitation wavelength of the green fluorescence was at 488 nm, and its emission window was 500−550 nm. Scale bar = 20 μm.

To confirm the selectivity of CFT for $O_2^{\bullet-}$/pH, we examined the fluorescent responses in the presence of competing ROS, reactive nitrogen species (RNS) and media formulations of various pH. As shown in Figure S3, the blue fluorescence CFT signal exhibited high selectivity for $O_2^{\bullet-}$ and the green fluorescence for pH. Generally, these results demonstrate that the caffeoyl-based and fluorescein-based recognition sites can exclusively respond to $O_2^{\bullet-}$ or pH, respectively.

We next investigated the fluorescence response time and reversibility of CFT regarding $O_2^{\bullet-}$/pH. As shown in Figure S4, CFT displayed rapid real-time detection of $O_2^{\bullet-}$/pH. Moreover, the fluorescence signal was maintained for 50 min, which indicated superior photostability. Furthermore, CFT exhibits a reversible on−off-on mechanism and instantaneous fluorescence responses toward the alternate addition of $O_2^{\bullet-}$/ ascorbic acid or acid/base medium. In addition, we determined that CFT did not induce marked cytotoxicity at concentrations below 5.1 mM (Figure S5). These results suggest that CFT can serve as a robust sensor to realize dynamic fluorescence imaging for $O_2^{\bullet-}$ and pH levels and affords an excellent opportunity for real-time examination of the cross-talk between these two systems in biological specimens.

We proceeded to evaluate the biological feasibility of CFT in live cells by means of *in situ* fluorescence imaging. In this experiment, 2-methoxyestradiol (2-ME), which is an effective $O_2^{\bullet-}$-producing agent, was used to elevate $O_2^{\bullet-}$ concentrations.[25] Figure 2A2,A4 illustrates that 4T1 cells treated with 2-ME (1.0 μg/mL) exhibited strong blue fluorescence in comparison with the control without 2-ME. These images indicated significant elevations in $O_2^{\bullet-}$ concentrations. Next, after adding 1.0 mM ascorbic acid to these cells, the blue fluorescence decreased immediately, which indicated decreased $O_2^{\bullet-}$ concentrations. Furthermore, other reversible fluorescent changes were observed following the successive treatment of 4T1 cells with 2-ME and then ascorbic acid. Additionally, the specificity of CFT for $O_2^{\bullet-}$ was further confirmed by adding a superoxide scavenger (Tiron, 10 μM). The high K^+ concentration buffer and ionophore nigericin were utilized to vary pH levels within cells. Figure 2B,D shows that the CFT fluorescence intensities of 4T1 cells were enhanced along with increasing pH values (6.5−9.0), whereas the fluorescence weakened with pH values declining to 7.0. Subsequently, the other reversible fluorescent changes were observed from pH 7.0 to 9.0. Collectively, the imaging results suggest that CFT is able to real-time visualize the transient changes of $O_2^{\bullet-}$ and pH in mitochondria of living cells.

Whether CFT could specifically target the mitochondria was next investigated. Mitochondria fluorescence colocalization experiments in 4T1 cells were carried out using CFT and MitoTracker Deep Red (Invitrogen). Figure 3 shows that the CFT fluorescent images merged well with those obtained using the commercial mitochondrial dye, and the Pearson's colocalization coefficient for the correlation of the brightness distribution between CFT and MitoTracker Deep Red was 0.93. These data provide strong evidence that the probe predominantly accumulates in mitochondria.

DOI: 10.1021/acs.analchem.7b01290
Anal. Chem. 2017, 89, 6840−6845

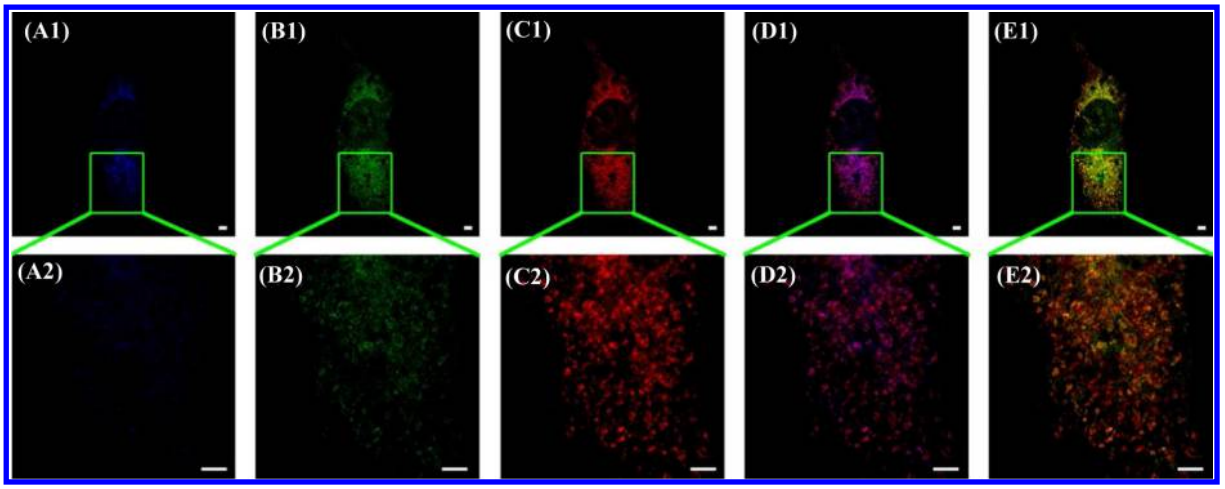

Figure 3. Intracellular localization of 10 μM CFT and 50 nM MitoTracker Deep Red in 4T1 cells with 1.0 μg/mL 2-ME (1.0 μg/mL) and the ionophore nigericin for 30 min (pH = 9.0 buffer). (A, B) Confocal images from CFT on blue and green channels (λ_{ex} = 405 nm, λ_{em} = 430−480 nm and λ_{ex} = 488 nm, λ_{ex} = 500−550 nm). (C) Confocal images from MitoTracker Deep Red on red channels (λ_{ex}= 633 nm, λ_{ex} = 650−700 nm). (D) Merged images of parts A and C. (E) Merged images of parts B and C. (A2−E2) Enlarged images from parts A1−E1. Scale bar = 2 μm.

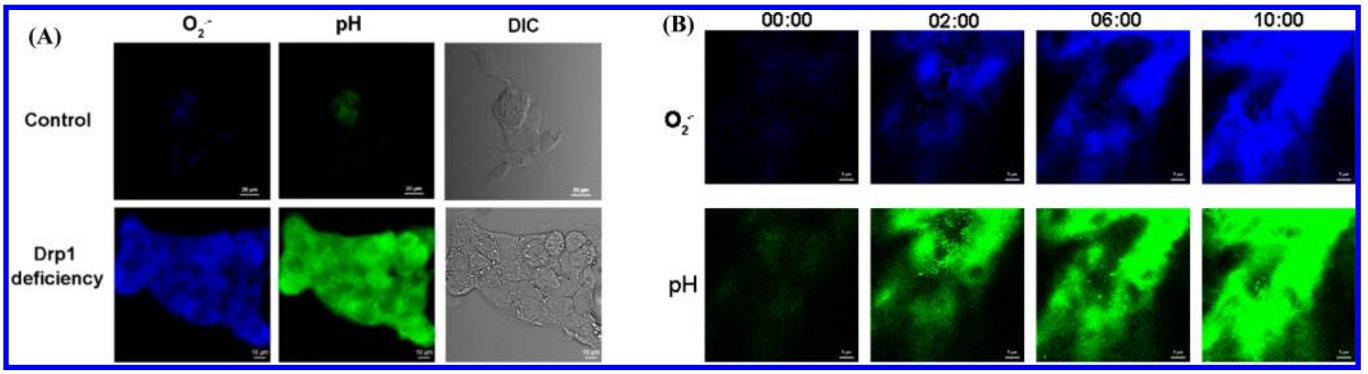

Figure 4. *In situ* fluorescence imaging in 4T1 cells and tumor-bearing mouse. (A) Drp1-deficient 4T1 cells were imaged by staining with 10 μM CFT for 10 min. The excitation wavelength of blue fluorescence was excited at 405 nm, and its emission window was 430−480 nm. The excitation wavelength of the green fluorescence was at 488 nm, and its emission window was 500−550 nm. Scale bar = 50 μm. (B) Time-dependent two-photon fluorescence images of a tumor-bearing mouse pretreated with 10 μM CFT and 100 μM mdivi-1. Images using a Zeiss microscope were recorded for up to 10 min. Fluorescence images from the blue channel and green channel were excited at 800 nm, and the emission window was collected at 430−480 nm and 500−550 nm, respectively. Scale bar = 20 μm (A) and 5 μm (B).

Hyperfused mitochondrial accumulations induced by Drp1 deficiency can cause apoptosis of cancer cells.[4] Since $O_2^{\bullet-}$ and pH play important roles in mitochondrial dysfunction, we investigate the real-time performance of $O_2^{\bullet-}$ and pH in hyperfused mitochondria to uncover the relevant mechanism. We knocked down expression of the mitochondrial fission protein Drp1 using siRNA in breast cancer cells.[26] Figure 4A shows that the blue and green fluorescence within 4T1 cells markedly increased following the loss of Drp1. These suggest that Drp1 deficiency in 4T1 cells induces an increase in $O_2^{\bullet-}$ and a significant increase in pH. In addition, a small-molecule Drp1 inhibitor[27] (mdivi-1, 100 μmol/L) was utilized to investigate $O_2^{\bullet-}$ and pH levels. Similar results were observed in that green and blue fluorescence was enhanced dramatically over time upon the addition of mdivi-1 (Figure 5A). The increase in $O_2^{\bullet-}$ levels and the synchronous pH elevation were responsible for the increased fluorescence intensities of CFT. At the same time, the mitochondria hyperfused into irregular shapes 2−3 μm in size and eventually underwent apoptosis. As shown in Figure S6, knock down of Drp1 enhanced the production of pro-apoptotic Bax and caspase-3 proteins while reducing the expression of antiapoptotic Bcl-2. These results suggest that 4T1 cells undergo apoptosis following mitohyperfusion, and these events are associated with increases in $O_2^{\bullet-}$ and pH levels. Obviously, both $O_2^{\bullet-}$ and pH increasing in mitochondrial hyperfusion are closely associated with apoptosis of breast cancer cells.

To further establish whether these signaling pathways operate in animals, we utilized CFT to visualize changes in $O_2^{\bullet-}$ levels and pH in mice (Figure 4B and Figure S8). After an injection of 100 μM mdivi-1, both the blue and green fluorescence signals become increasingly bright within 10 min. These images clearly demonstrated increased [$O_2^{\bullet-}$] and pH levels induced by Drp1 deficiency. The advantageous fluorescent properties of the TP probe allowed us to obtain *in situ* images of the $O_2^{\bullet-}$ and pH levels to a depth of 1.35 cm into the murine tumor tissue. Altogether, the experimental results further confirm the intimate relationships between mitochondrial hyperfusion and $O_2^{\bullet-}$/ pH fluctuations *in vivo*.

Although we had observed $O_2^{\bullet-}$/pH increases in the hyperfused mitochondria, the main source of the excessive $O_2^{\bullet-}$ following the loss of Drp1 was still unclear. Therefore, the mitochondrial respiratory complex, xanthine oxidase, and cyclooxygenase were considered as potential sources to investigate

DOI: 10.1021/acs.analchem.7b01290
Anal. Chem. 2017, 89, 6840−6845

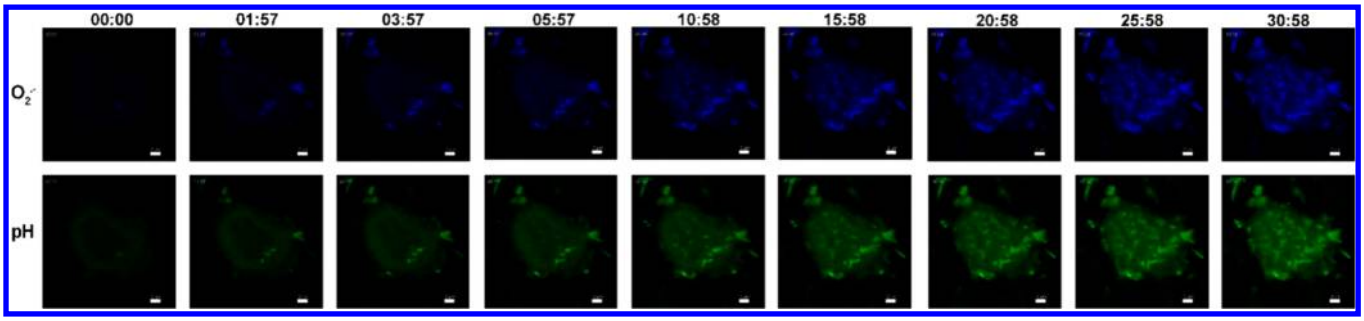

Figure 5. Time-dependent images of 4T1 cells pretreated with 10 μM CFT and 100 μM mdivi-1. Scale bar = 2 μm. The excitation wavelength of blue fluorescence was excited at 405 nm, and its emission window was 430−480 nm. The excitation wavelength of the green fluorescence was at 488 nm, and its emission window was 500−550 nm.

the underlying mechanism of $O_2^{\bullet-}$ and pH fluctuations induced by Drp1 deficiency. Figure S7a shows that the $O_2^{\bullet-}$ and pH levels in Drp1-deficient cells decreased following treatment with complex I and II inhibitors. In contrast, the other enzyme inhibitors did not disturb $O_2^{\bullet-}$ or pH levels. The fluorescent variations indicated that complexes I and II regulated $O_2^{\bullet-}$ and pH levels in Drp1-deficient cells. To confirm these observations, mdivi-1 treatment was used to investigate the signaling cascades (Figure S7b). The identical results demonstrated that mitochondrial complexes I and II regulate $O_2^{\bullet-}$ and pH fluctuations in Drp1-deficient cells and might play an important role in the apoptosis of breast cancer cells.

Although McBride and colleagues have described the importance of intracellular redox conditions in regulating mitochondrial fusion,[28] the changes of $O_2^{\bullet-}$ and pH in hyperfused mitochondria determining breast cancer fate are basically unknown. To address these issues, we have developed a visualization tool to investigate $O_2^{\bullet-}$ and pH signals induced by mitohyperfusion. Our experiments showed that $O_2^{\bullet-}$ and pH enhancements are key factors in the signal transduction pathway triggered by Drp1 inactivation for breast cancer cell apoptosis, and the mitochondrial electron-transport chain complexes I and II are the main sources of $O_2^{\bullet-}$. Furthermore, some studies[29] showed that $O_2^{\bullet-}$ reacts with reduced glutathione (GSH) to cause an increase in oxygen consumption and oxidized glutathione (GSSG) formation, which is an essential determinant of mitochondrial fusion. Meanwhile, Mitofusion 1 (Mfn1) and Mitofusion 2 (Mfn2), which are required for fusion, accumulate within the cells. The redox imbalance also causes the delivering of mitochondrial cytochrome c (Cyt C) to the cytosol[30] and pro-apoptosic proteins increase. The final response is that mitochondria hyperfusion and the breast cancer cells undergo apoptosis (Figure 6).

CONCLUSION

In summary, with the demand for revealing the roles of $O_2^{\bullet-}$ and pH in mitochondrial hyperfusion for cancer treatment, we have developed a TP fluorescent probe, which has the following advantages: (1) specifically recognizing $O_2^{\bullet-}$ and pH with corresponding distinct fluorescent signals and single excitation-dual emission; (2) responding to $O_2^{\bullet-}$ and pH instantaneously, dynamically and reversibly; (3) precisely locating the mitochondria; and (4) possessing favorable TP fluorescence properties for higher temporal resolution, deeper penetration, and reduced background interference. Crucially, with the assistance of this desirable probe, we determined the transient variations of $O_2^{\bullet-}$ and pH levels in hyperfused mitochondria. Our results showed that

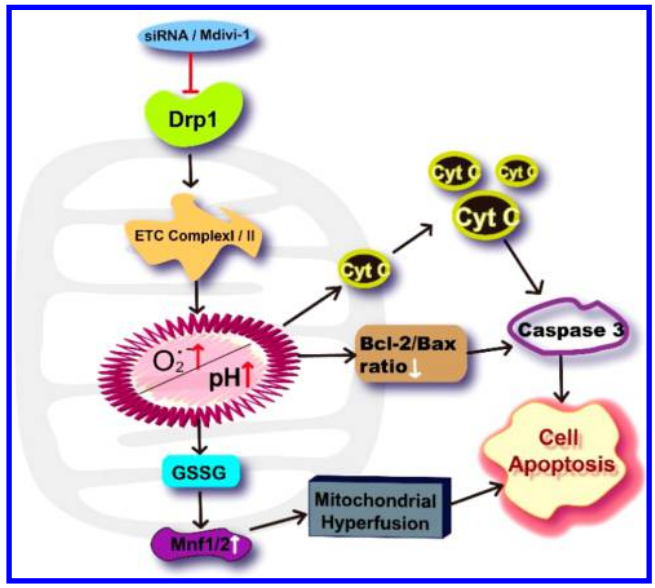

Figure 6. Our working model shows that that the apoptosis in breast cancer cells is induced by increases in $O_2^{\bullet-}$ and pH triggered by deficiency of the fission protein Drp1.

Drp1-deficiency transduce a signal through mitochondrial complexes I and II to increase $O_2^{\bullet-}$ and pH levels and eventually causes mitochondrial hyperfusion and apoptosis of 4T1 cells. Together, these data indicate that CFT provides a robust tool for unveiling the roles of $O_2^{\bullet-}$ and pH in signals associated with mitochondrial dysfunction in cells and *in vivo*.

ASSOCIATED CONTENT

Supporting Information

The Supporting Information is available free of charge on the ACS Publications website at DOI: 10.1021/acs.analchem.7b01290.

Additional experimental data, including synthesis, characterization, photophysical properties, cytotoxicity, and experimental details (PDF)

AUTHOR INFORMATION

Corresponding Authors

*E-mail: tangb@sdnu.edu.cn. Fax: (86)531-86180017.
*E-mail: lip@sdnu.edu.cn.

ORCID

Bo Tang: 0000-0002-8712-7025

Notes

The authors declare no competing financial interest.

DOI: 10.1021/acs.analchem.7b01290
Anal. Chem. 2017, 89, 6840−6845

■ ACKNOWLEDGMENTS

This work was supported by 973 Program (Grant 2013CB933800), National Science Foundation of China (Grants 21390411, 21535004, 21227005, 21475079, and 21675105), and the Program for Changjiang Scholars and Innovative Research Team in University.

■ REFERENCES

(1) Santel, A.; Fuller, M. T. *J. Cell Sci.* **2001**, *114*, 867−874.
(2) Smirnova, E.; Griparic, L.; Shurland, D. L.; van der Bliek, A. M. *Mol. Biol. Cell* **2001**, *12*, 2245.
(3) Chen, H.; Chan, D. C. *Hum. Mol. Genet.* **2009**, *18*, R169.
(4) Manczak, M.; Reddy, P. H. *Hum. Mol. Genet.* **2012**, *21*, 2538.
(5) Rehman, J.; Zhang, H. J.; Toth, P. T.; Zhang, Y.; Marsboom, G.; Hong, Z.; Salgia, R.; Husain, A. N.; Wietholt, C.; Archer, S. L. *FASEB J.* **2012**, *26*, 2175.
(6) Dumont, M.; Beal, M. F. *Free Radical Biol. Med.* **2011**, *51*, 1014.
(7) Finkel, T. *Curr. Opin. Cell Biol.* **1998**, *10*, 248.
(8) Yang, J.; Liu, X.; Bhalla, K.; Kim, C. N.; Ibrado, A. M.; Cai, J.; Peng, T. I.; Jones, D. P.; Wang, X. *Science* **1997**, *275*, 1129.
(9) Takahashi, A.; Masuda, A.; Sun, M.; Centonze, V. E.; Herman, B. *Brain Res. Bull.* **2004**, *62*, 497.
(10) Shibanuma, M.; Kuroki, T.; Nose, K. *J. Cell. Physiol.* **1988**, *136*, 379.
(11) Hu, J. J.; Wong, N. K.; Ye, S.; Chen, X.; Lu, M. Y.; Zhao, A. Q.; Guo, Y.; Ma, A. C.; Leung, A. Y.; Shen, J. *J. Am. Chem. Soc.* **2015**, *137*, 6837.
(12) Li, Y.; Wang, Y.; Yang, S.; Zhao, Y.; Yuan, L.; Zheng, J.; Yang, R. *Anal. Chem.* **2015**, *87*, 2495.
(13) Gao, X.; Ding, C.; Zhu, A.; Tian, Y. *Anal. Chem.* **2014**, *86*, 7071.
(14) Li, P.; Zhang, W.; Li, K.; Liu, X.; Xiao, H.; Zhang, W.; Tang, B. *Anal. Chem.* **2013**, *85*, 9877.
(15) Kim, H. J.; Heo, C. H.; Kim, H. M. *J. Am. Chem. Soc.* **2013**, *135*, 17969.
(16) Rajadhyaksha, M.; Grossman, M.; Esterowitz, D.; Webb, R. H.; Anderson, R. R. *J. Invest. Dermatol.* **1995**, *104*, 946.
(17) Brunoud, G. *Nature* **2012**, *482*, 103.
(18) Zhou, L.; Zhang, X.; Wang, Q.; Lv, Y.; Mao, G.; Luo, A.; Wu, Y.; Wu, Y.; Zhang, J.; Tan, W. *J. Am. Chem. Soc.* **2014**, *136*, 9838.
(19) Zhang, W.; Wang, X.; Li, P.; Huang, F.; Wang, H.; Zhang, W.; Tang, B. *Chem. Commun.* **2015**, *51*, 9710.
(20) Fan, J.; Han, Z.; Kang, Y.; Peng, X. *Sci. Rep.* **2016**, *6*, 6.
(21) Mao, G. J.; Wei, T. T.; Wang, X. X.; Huan, S.; Lu, D. Q.; Zhang, J.; Zhang, X. B.; Tan, W.; Shen, G. L.; Yu, R. Q. *Anal. Chem.* **2013**, *85*, 7875.
(22) Zhang, W.; Li, P.; Yang, F.; Hu, X.; Sun, C.; Zhang, W.; Chen, D.; Tang, B. *J. Am. Chem. Soc.* **2013**, *135*, 14956.
(23) Breeuwer, P.; Drocourt, J.; Rombouts, F. M.; Abee, T. *Appl. Environ. Microbiol.* **1996**, *62*, 178−183.
(24) Dickinson, B. C.; Srikun, D.; Chang, C. J. *Curr. Opin. Chem. Biol.* **2010**, *14*, 50−56.
(25) Lakhani, N. J.; Sarkar, M. A.; Venitz, J.; Figg, W. D. *Pharmacotherapy* **2003**, *23*, 165.
(26) Qian, W.; Choi, S.; Gibson, G. A.; Watkins, S. C.; Bakkenist, C. J.; Van, H. B. *J. Cell Sci.* **2012**, *125*, 5745−5757.
(27) Cui, M.; Tang, X.; Christian, W. V.; Yoon, Y.; Tieu, K. *J. Biol. Chem.* **2010**, *285*, 11740.
(28) Shutt, T.; Geoffrion, M.; Milne, R.; Mcbride, H. M. *EMBO Rep.* **2012**, *13*, 909.
(29) Winterbourn, C. C.; Metodiewa, D. *Arch. Biochem. Biophys.* **1994**, *314*, 284.
(30) Cai, J.; Yang, J.; Jones, D. P. *Biochim. Biophys. Acta, Bioenerg.* **1998**, *1366*, 139.

DOI: 10.1021/acs.analchem.7b01290
Anal. Chem. 2017, 89, 6840−6845